A BENCHMARK PROBLEM OF INDUCTION HEATING ANALYSIS

P. Di Barba[1], M.E. Mognaschi[*1], D.A. Lowther[1,2],
F. Dughiero[3], M. Forzan[3], S. Lupi[3], E. Sieni[3]

[1]Department of Electrical, Computer and Biomedical Engineering, University of Pavia,
Via Ferrata, 5, 27100 Pavia, Italy
[2]Department of Electrical and Computer Engineering, McGill University,
3480 University Street, Montreal, QCH3A0E9 Canada
[3]Department of Industrial Engineering, Padova University,
Via Gradenigo,6/a, 35131 Padova, Italy

ABSTRACT. In the paper, a benchmark in the area of induction heating is presented in order to test methods and codes of field analysis in a comparative way. In particular, the transient thermal analysis of a magnetic steel cylindrical billet is considered: the coupled-field problem is characterized by a twofold non linearity, *i.e.* the dependence of magnetic permeability on both field strength and temperature.

INTRODUCTION

In the community of computational electromagnetics, the set of benchmark problems proposed by the TEAM (Testing Electromagnetic Analysis Methods) series of workshop is a reference for testing numerical methods in a comparative way [1]. Nevertheless, there is a lack of benchmarks specifically focused on induction heating devices, as far as numerical modelling is concerned. In [2,3,4] a benchmark of induction heating was proposed, but the attention was on the inverse problem related to inductor optimization rather than on the direct problem of field analysis. In fact, computational induction heating problems are challenging because they involve different physical domains; therefore, the development of non-linear coupled-field models and the consequent choice of suitable solvers are mandatory[5]. Too often commercially available numerical solvers, *e.g.* the finite-element ones, are used as general-purpose black boxes.

Moving from this background, it is here proposed a benchmark of coupled-field analysis. The problem is a classical one, well known in industrial applications of induction heating: it deals with the transient thermal analysis of a steel cylindrical billet, subject to a time varying magnetic field produced by a multi-turn inductor coil [6].

It is an example showing that even in case of quite simple geometries complex analysis problems may arise.

The solution of induction heating coupled electromagnetic and thermal problem is usually carried out by resorting to a weak coupling scheme, solving independently the Maxwell's equations in sinusoidal steady-state and Fourier's equation time dependent by a suitable algorithm, e.g. Euler or Crank-Nicolson, that subdivides the process time in several time-steps. The coupling terms are the spatial distribution of the Joule's losses, calculated by solving the Electro-Magnetic (EM) problem and applied as source of thermal problem, and the temperature field, calculated by solving the transient thermal problem, that modifies the material properties dependant on temperature at each time step. The time constants that characterize the natural response of the EM and Thermal (TH) problems, respectively, differ

of orders of magnitude, and this allows to independently solve the electromagnetic and thermal equations.

The main aim of this work is to discuss the impact of different models applied to describe the dependence of the magnetic permeability on the magnetic field as well as the temperature, even if several different choices regarding the numerical model may affect the result quality, like e.g. mesh dimension, duration of time steps, and description of thermal losses.

DEVICE DESCRIPTION

The device under study is composed of a solenoidal inductor coil and a coaxial cylindrical steel billet with the same axial length.

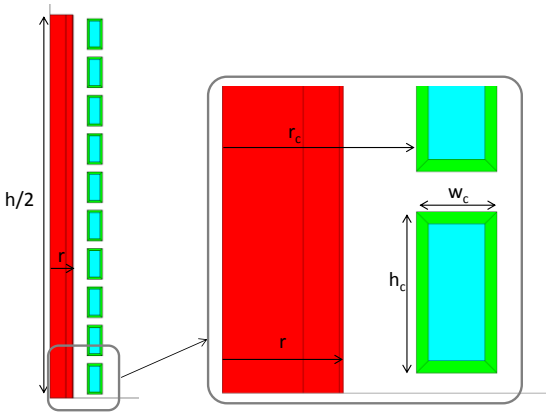

Figure 1. Inductor-load system geometry of the benchmark

Geometry

With reference to the symbols of Fig. 1, the geometrical data of the benchmark induction heating system are those summarized in Table 1.

The inductor coil is composed of 20 circular turns, made of copper tube, series connected and uniformly spaced along the Y axis.

Table 1.Numerical data of the model geometry

Parameter	Description	Value [mm]
h	Billet axial length	1000
h_{coil}=h	Inductor coil axial length	1000
r	Billet external radius	30
r_c	Inductor coil internal radius	48
h_c	Coil turn axial length	40
w_c	Coil turn radial width	20
t_c	Copper turn conductor thickness	3

Material properties

The billet is made of C45 steel, whose material properties, specific heat capacity, thermal conductivity and electrical conductivity, are given in Fig. 2 (a), (b) and (c) as a function of temperature.

Fig. 2 (d) gives the B-H curve of the steel at 20 °C, assumed as a given (experimental) data in the benchmark. To this curve correspond the values of the relative permeability μ_{20} at 20 °C of Table 2.

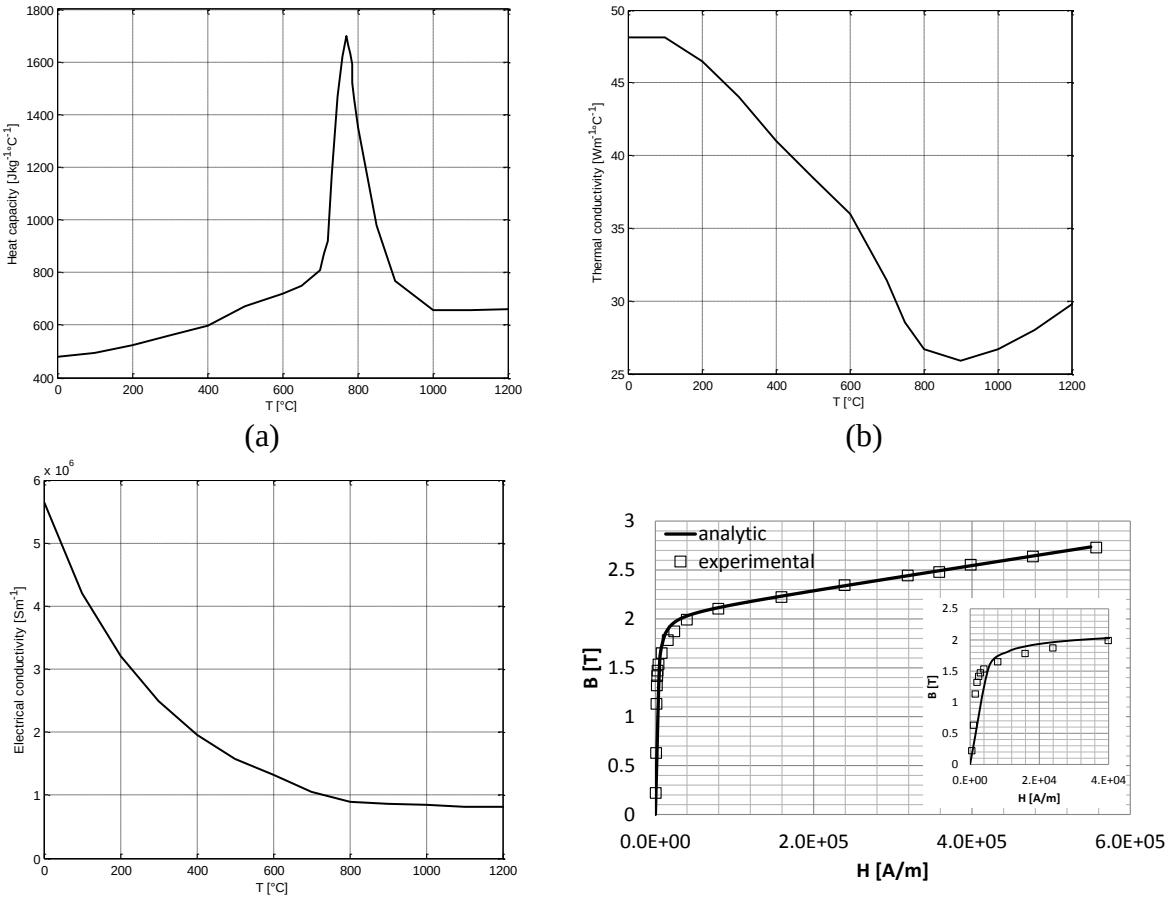

Figure 2. Material properties of steel C45: (a) specific heat capacity c_p, (b) thermal conductivity λ, (c) electrical conductivity σ as a function of temperature; (d) B-H curve at T=20 °C implemented in Model A

Table 2. Relative permeability μ_{20} at T=20°C.

H [Am^{-1}]	0	500	1000	1500	2000	2500	3000
μ_{20}	0	350	500	600	525	450	390
H [Am^{-1}]	4000	8000	15900	23900	39900	79700	159400
μ_{20}	305	164	89.2	62.3	39.7	21	11.1
H [Am^{-1}]	239100	318800	358700	398500	477000	557000	
μ_{20}	7.8	6.1	5.5	5.1	4.4	3.9	

However, permeability is strongly dependent also on temperature and its correct description is a very critical point for modelling the heating transient near the Curie temperature.

"In fact variations of magnetic permeability with temperature are a very complicated problem and information about it is quite insufficient, especially for "industrial" steels typically used in induction heating processes, such as carbon and low alloyed steels [7].

The analysis of literature shows that in low magnetic fields the permeability drops with temperature much slower than in the strong fields" [8,9,10,11].

Therefore, in the benchmark two different models are proposed, used in some well-known numerical packages, for describing the non-linear variations of the B-H curve with temperature [12,13,14].

In view of collecting and comparing the results obtained by various authors with different

numerical methods, future contributors will make a choice between the B-H models here proposed depending on the package and the solver used.

The two models of non-linear permeability proposed for the benchmark are the following.

Model A

The relative magnetic permeability μ_r is approximated with the formula:

$$\mu_r(T,H) = 1 + f(T)\cdot\mu_{20}(H) \tag{1}$$

where μ_{20} is the field-dependent relative permeability at room temperature T=20°C, and the function f(T) is calculated with the relationships:

$$\begin{cases} f(T) = 1 - e^{\left(\frac{T-T_C}{C}\right)}, \; T < T_1, \; T_1 = T_c + C\ln 0.9 \\ f(T) = e^{\left(\frac{10(T_2-T)}{C}\right)}, \; T > T_1, \; T_2 = T_1 + 0.1C\ln 0.1 \end{cases} \tag{2}$$

The constant C is usually selected by users for fitting the approximated curve with experimental data. In the benchmark the value C=20 °C and the Curie temperature T_c = 770 °C have been chosen in order to fit with the given B-H curve of Fig. 2 (d) via (1).

Another way of approximating the given (experimental) B-H curve is based on the following relationship:

$$B(H) = \mu_0 H + B_s \frac{H_a + 1 - \sqrt{(H_a+1)^2 - 4H_a(1-a)}}{2(1-a)} \tag{3}$$

with $H_a = \mu_0 H(\mu_{r,i} - 1)B_s^{-1}$.

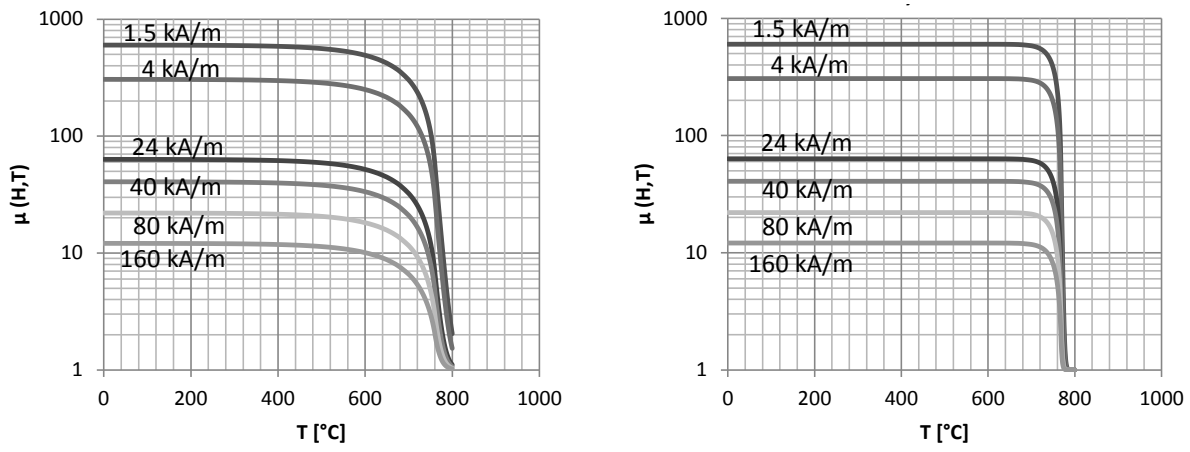

(a) (b)

Figure 3. Relative magnetic permeability as function of temperature and magnetic field strength according to eqns.(1) and (2) [(a) C=100; (b) C=20]

In this model the relative magnetic permeability is described by means of its initial value $\mu_{r,i}$, the saturation value of the induction field B_s of 2.05 T and a knee adjusting coefficient, *a*. The temperature dependence is again given by eqns.(1)-(2).

The given B-H curve can be approximated by eqn. (3) with the triplet of parameters $\mu_{r,i}$=600, B_s = 2.05 T and a=0.5. The temperature dependence is again given by eqn. (2).

Using equations (1) and (2) families of permeability dependent on temperature and magnetic field strength can be drawn (Fig. 3).

Model B

The relative magnetic permeability μ_r is modelled as a function of magnetic field strength H and temperature T by the relationship:

$$\mu_r(T,H) = 1 + (\mu_r(H) - 1)\left(1 - \left(\frac{T}{T_c}\right)^{\alpha}\right) \tag{4}$$

where T_c is set at 770 °C and α is a parameter selected by the user [13]. The influence of α on $\mu_r(T,H)$ is shown in figure 4.

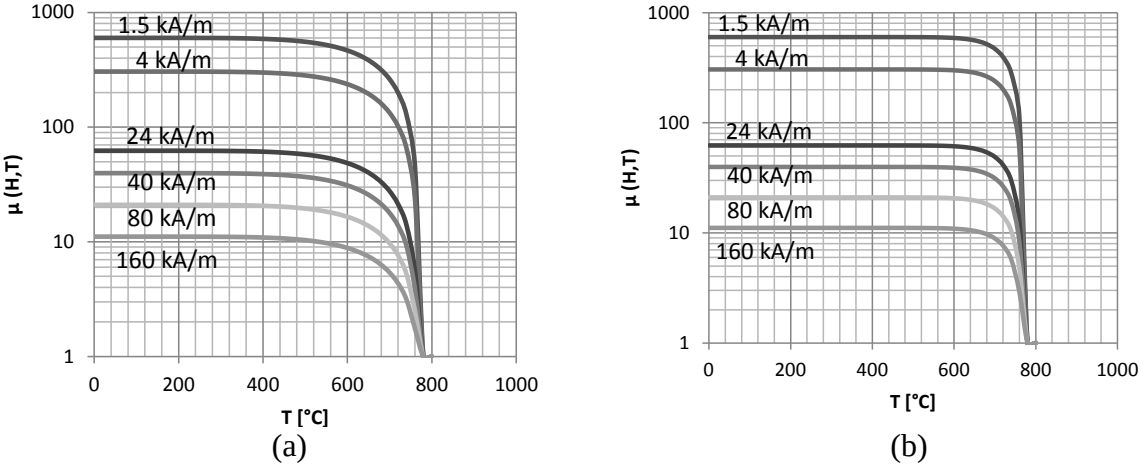

Figure 4. Relative magnetic permeability as function of temperature and magnetic field strength according to eqn. (4) [(a) α=6; (b) α=16]

FIELD ANALYSIS

The EM and TH problems can be solved using a 2D axisymmetric model. The EM problem is solved in time-harmonic conditions, whereas the TH one is solved in transient conditions with thermal sources due to the power density induced in the billet. The electromagnetic domain is composed of half of the inductor, half of the billet and surrounding air, whereas the thermal one is composed only of half of the billet. The inductor is assumed to be supplied at 2 kHz with a sinusoidal current with amplitude of 3,500 A_{rms}. This assumption corresponds to a current driven supply; alternatively, a voltage driven supply can be assumed, but in this case the model equation should incorporate the circuit equations relating the supply voltage to the winding current.

The electromagnetic and thermal problems are coupled because most of the material properties of C45 steel are temperature dependent, and permeability depends both on temperature and field strength; hence, at each time step of the transient thermal analysis, a time-harmonics electromagnetic analysis must be solved too.

Electromagnetic problem

The electromagnetic 2D problem can be solved using the A-V formulation. The analysis of the magnetic problem is solved in terms of the phasor of the magnetic vector potential, A, coupled with the phasor of the electric scalar potential, V. The following coupled second order PDEs are originated:

$$\nabla \times \mu^{-1} \nabla \times \dot{\mathbf{A}} + \mathrm{j}\omega\mu\sigma\dot{\mathbf{A}} = -\sigma \nabla \dot{V} + \dot{\mathbf{J}}_S \tag{5}$$

$$\nabla \cdot \sigma(\mathrm{j}\omega\mu \dot{A} + \nabla \dot{V}) = 0 \tag{6}$$

where $\mu=\mu_o\mu_r$ is the material permeability, ω field pulsation, σ electrical conductivity and $\dot{\mathbf{J}}$ and $\dot{\mathbf{A}}$ are the phasors of the current density and magnetic vector potential, respectively. Equation (5) is the equation governing the magnetic field, while equation (6) makes the total current to be solenoidal. Homogeneous Neumann boundary conditions are set along y=0, while homogeneous Dirichlet conditions are forced elsewhere. The rectangular air box incorporating the device was truncated at a suitable distance from the device axes.
The solution of a sinusoidal steady state problem in terms of phasorial quantities requires that all the quantities are iso-frequential sinusoids. This assumption fails when the magnetic induction exhibits a nonlinear dependence from magnetic field. Usually the EM solution in a nonlinear model considers a modified BH curve calculated in order to keep energetic equivalence between the real nonlinear model and the equivalent one [15].

Thermal problem

The thermal problem solves the Fourier equation:

$$\rho c_p \frac{\partial T}{\partial t} - \nabla \cdot (\lambda \nabla T) = \sigma \omega^2 \left\| \dot{A} \right\|^2 \tag{7}$$

with T unknown temperature, ρ mass density, c_p specific heat capacity and λ thermal conductivity. The boundary conditions are:

$$n \cdot (\lambda \nabla T) = 0 \quad \text{on } y = 0 \text{ and } x = 0 \tag{8}$$

$$n \cdot (\lambda \nabla T) = \alpha_c \cdot (T_{ext} - T) \tag{9}$$

where α_c is the convective exchange coefficient assumed equal to 7 $Wm^{-2}K^{-1}$ and T_{ext} the external temperature equal to 70°C along lateral surface of the billet (x = r = 3 cm), while T_{ext} = 25°C for the end surface (y = h/2 = 50 cm) and

$$n \cdot (\lambda \nabla T) = \varepsilon k_B (T_{ext}^4 - T^4) \tag{10}$$

where ε is the emissivity coefficient equal to 0.8, k_B the Stefan-Boltzmann constant and T_{ext} = 70 °C for the lateral surface (x = r = 3 cm), while T_{ext} = 25°C for the end surface (y = h/2 = 50 cm).

METHODS AND NUMERICAL SOLVERS

Different numerical methods have been used to solve the field problem: the finite difference method (ELTA code [14]) and the finite element method codes (MagNet by Infolytica [13] and Flux by Cedrat [12]).

For the electromagnetic problem solved with finite element method a 2D second-order mesh has been generated. A typical mesh exhibits 150,000 nodes and 75,000 elements in Flux model (Fig. 5), 775,000 elements in MagNet model.

In MagNet and FLUX the conjugate gradient method is used for solving the system of equations from the finite element model. When the matrix system is nonlinear, it has to be linearized before solving the system. For linearizing the system, the Newton Raphson method is used by MagNet and FLUX. The B-H curves of the C45 steel versus the temperature are given to MagNet in the range from 10 °C to 1500 °C with subintervals of 10 degrees. In each subinterval, the dependence of the B-H curve on temperature is considered by means of a

piecewise linear interpolation. The latter is obtained via a linear regression from equation (2), model A. In Flux the temperature dependent B-H curve is defined using equations (2) and (3). In ELTA the temperature dependent B-H curve is defined using equation (4).

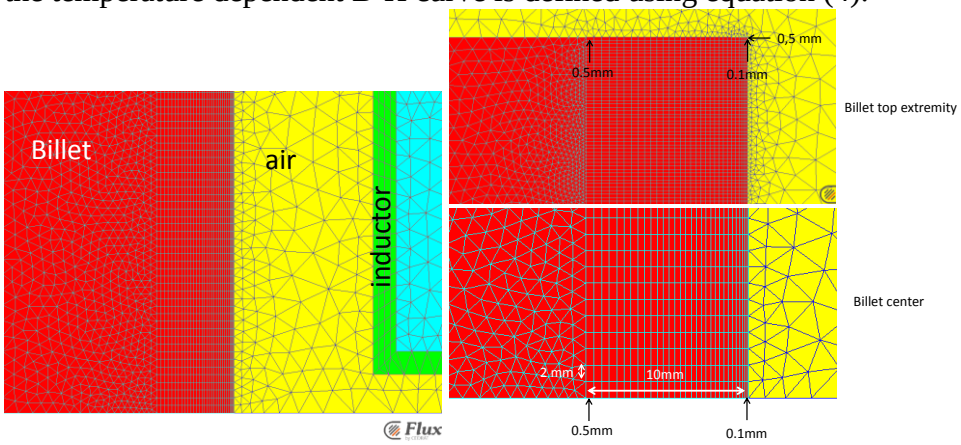

Figure 5. Typical mesh of the electromagnetic problem

COMPARISON OF RESULTS

Starting from the analysis of the curves of figures 3 and 4, model A and model B have been compared with values of C equal to 20 and 100, and α to 6 and 16 respectively.

Due to the shapes of Fig.s 3 and 4, the main differences in the results occur near the transition of Curie temperature, as shown in Fig. 6:

- Fig. 6 (a) gives the variations of power induced in the workpiece during the heating transient. With the two models the peaks of induced power occur at different time instants and have different values which depend on the choice of the model parameters; in particular, the peak values are nearly the same for C=20 and α=6.
- Fig. 6 (b) shows the corresponding transient temperature distributions

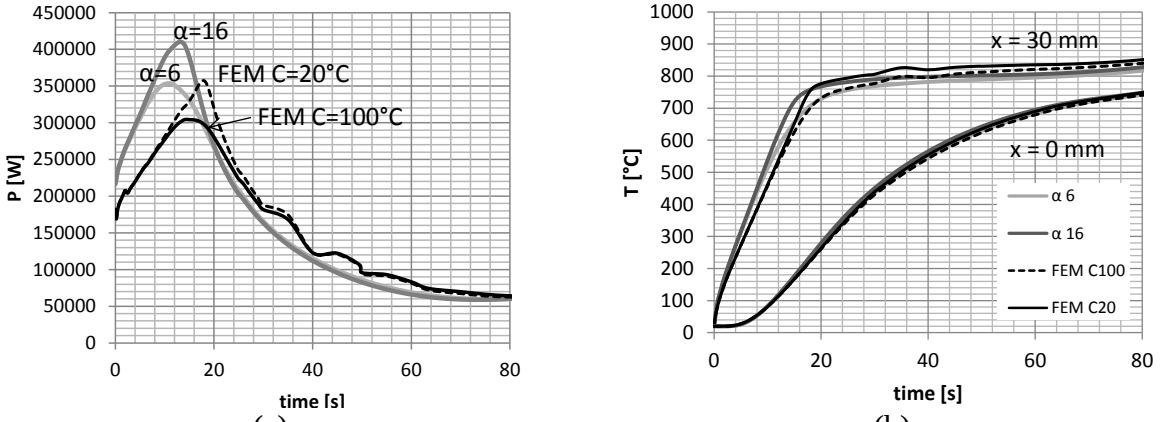

(a) (b)

Figure 6. Examples of results obtained with models A) and B) and different model parameters (a) induced power during heating; (b) corresponding transient temperature distribution

From these results a logical conclusion seems to propose for the benchmark the values C=20 in model A and α=6 in model B.

However, it should be noted that this choice has a certain influence only on power and temperature distributions near Curie point, but it has low influence on the final values of temperature and heating time at the end of the process. In fact, the total energies induced in the workpiece, calculated for A) and B) models, differ for less than 3% (see Table 3).

Table 3. Induced total energy equivalence for model A and B

	α = 6, mod B	α = 16, mod B	C = 20, mod A	C = 100, mod A
Energy $\cdot 10^7$ [J]	2.42	2.45	2.48	2.42

Effect of the mesh: Curie front movement and penetration depth

Because the magnetic relative permeability is strongly temperature dependent, in particular when it is close to the Curie temperature, it happens that, for some time instants, the billet material exhibits substantial changes of permeability value depending on the temperature. It behaves like a non-linear magnetic material in the region of the billet below the Curie temperature, while it behaves like a non-magnetic one in the region of the billet being above the Curie temperature. In Fig 7b the temperature profile versus the radius of the billet is shown for t =62.5 s: it can be noted that approximately one half of the billet is under the Curie temperature, while the other half is above it.
The space transition between the two regions depends on time, and it is critical from the numerical point of view. In fact, if the discretization is not enough refined, a ripple effect like the one shown in Fig. 7a might arise. The ripple can be eventually attributed to the very steep decrease of permeability around the Curie temperature.

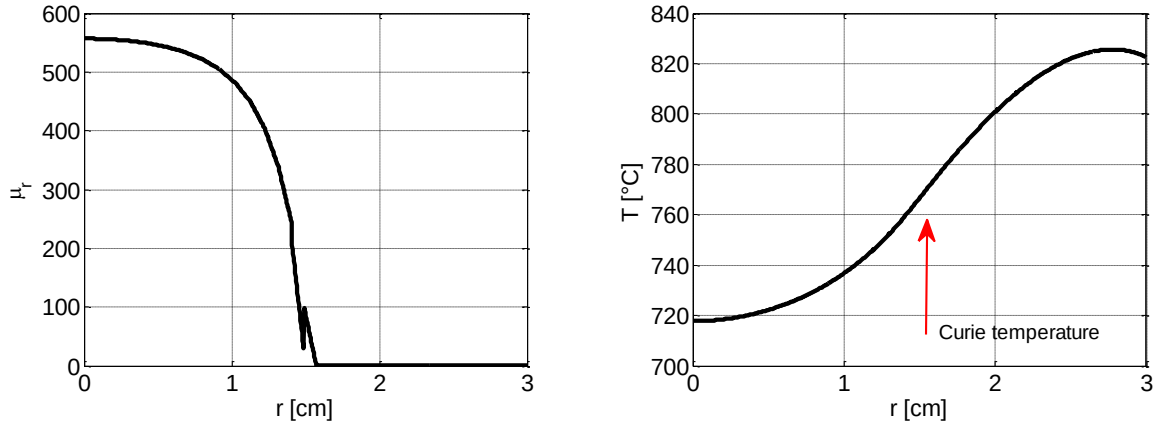

(a) (b)

Figure 7. Relative permeability versus radius of the billet (a) and temperature versus radius of the billet (b), at the time instant t = 62.5 s.

In order to save computational time, it could be effective to divide the billet domain into two regions: the one below the Curie temperature and the one above it. This way, two different penetration depth can be considered, namely δ_{cold} and δ_{hot} , respectively: δ_{cold} , related to the region below the Curie temperature, is lower than δ_{hot} related to the region above the Curie temperature. In turn. the penetration depth is temperature dependent because both electrical conductivity and magnetic permeability are temperature dependent.
Hence, the finite element mesh could be structured accordingly: below the Curie temperature the problem, especially the magnetic one, should be solved with high accuracy, hence the maximum element size of the mesh could be set to e.g. 0.5 δ_{cold} which is about 2 10^{-4} m. In contrast, in the region of the billet above the Curie temperature, the maximum element size of the mesh could be set to e.g. 2 δ_{hot}, which is about 1.1 10^{-2} m, as shown in Fig. 8.

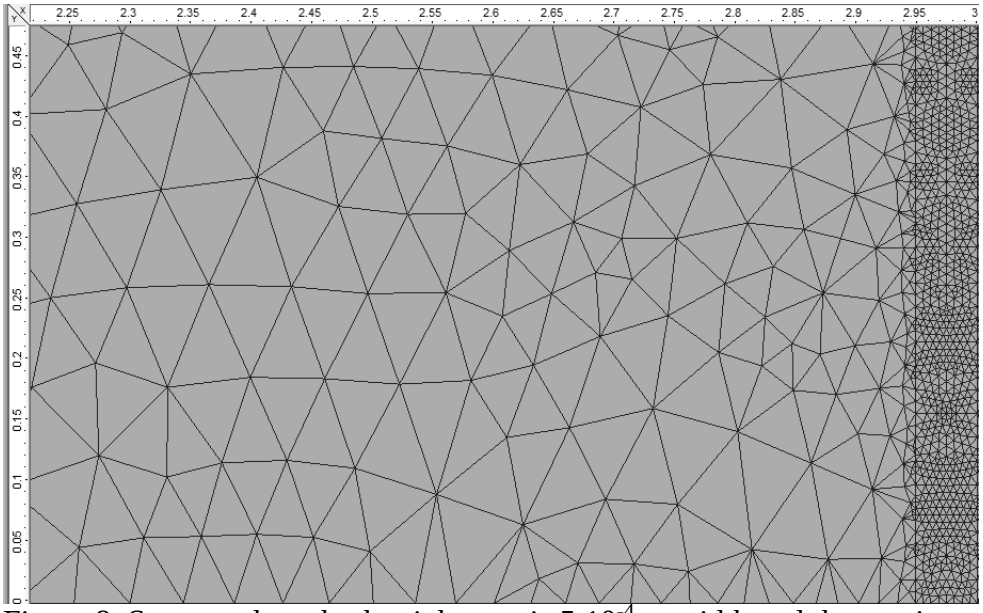

Figure 8. Structured mesh: the right part is 5 10^{-4} m width and the maximum element size is 6 10^{-5} m, the left part of the mesh has a maximum element size of 7 10^{-4} m.

Because the transition zone between the hot and the cold regions of the billet is time-varying, as shown in Fig. 9, it is necessary that the mesh of the billet is structured in space and updated in time in order to track the Curie front movement.

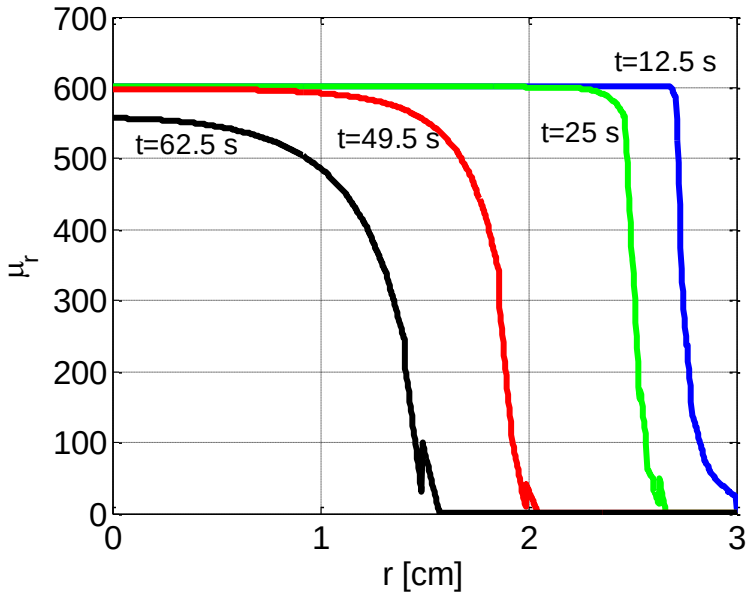

Figure 9. Relative permeability versus radius of the billet for different time instants: the ripple due to a coarse mesh identify the position of the Curie front, which is time-varying.

Unfortunately, this kind of mesh control is not usually implemented in the commercially licensed FE codes. Consequently, the maximum element size of the mesh should be set to 0.5 δcold in the whole billet; consequently, however, the extra load could be fatal in terms of runtime for field analysis.

CONCLUSIONS

In the paper a benchmark in the field numerical calculations of induction heating systems with magnetic loads is proposed. Scope of this benchmark is to define a simple reference example used for collecting and comparing results obtained by different authors with different numerical software. The results presented in the paper have shown that a critical point of calculations is the description of the variations of magnetic permeability with temperature and magnetic field strength. Solutions of the proposed benchmark with different numerical methods and results obtained by different authors are therefore welcome, in order to set up a reference collection of data in the area of computational induction heating.

REFERENCES

[1] www.compumag.org/jsite/team [last visit March 2016]

[2] Di Barba P., Dolezel I., Karban P., Kus P., Mach F., Mognaschi M. E., Savini A. (2013). Multiphysics field analysis and multiobjective design optimization: a benchmark problem. Inverse Problems in Science & Engineering IPSE, 22 (7), 1214-1225.

[3] Di Barba P., Dughiero F., Forzan M., Sieni E. (2015). Improved solution to a multi-objective benchmark problem of inverse induction heating. International Journal of Applied Electromagnetics and Mechanics, 49 (2), 279-288.

[4] Di Barba, P., Dughiero, F., Forzan, M., Sieni, E. (2015). Multiobjective design optimization of an induction heating device: a benchmark problem. International Journal of Applied Electromagnetics and Mechanics, 47 (4), 1003-1013.

[5] P. Di Barba, I. Dolezel, M.E. Mognaschi, A. Savini, P. Karban (2014). Non-linear multi-physics analysis and multi-objective optimization in electroheating applications. IEEE Transactions on Magnetics, 50 (2).

[6] Lavers J.D. (1983). Numerical solution methods for electroheat problems. IEEE Trans. On Magnetics, Vol. MAG-19, n.6, November 1983, 2566-2572

[7] Nemkov V., Goldstein R. (2016). Striation effect in induction heating: myths and reality. Proc. of HES-16, Padua, May 2016

[8] Kuvaldin A.B. (1976). Low temperature induction heating of steel. Ed. Energija, Moskow, 111 p. (in Russian)

[9] Nemkov V.S. (2015). How accurate is computer simulation of induction heating? Proc. of EPM 2015 conference, Cannes, France.

[10] Zedler T., Nikanorov A., Nacke B. (2008). Investigation of relative magnetic permeability as input data for numerical simulation of induction surface hardening. Int. Scientific Coloquium MEP 2008, Hanover.

[11] Vladimirov S.N, Zeman S.N., Ruban V.V. (2009). Analytical approximations of thermal dependence of permeability of construction steels. Proc. of Tomsk univ., v.31.

[12] www.cedrat.com [last visit March 2016]

[13] www.infolytica.com [last visit June 2016]

[14] Nemkov V., Bukanin V., Zenkov A. (2010). Learning and teaching induction heating using the program ELTA. Proc. HES-10, Padua, May 18-21, 99-106.

[15] Canova, A., Dughiero, F., Fasolo, F., Forzan, M., Freschi, F., Giaccone, L., Repetto, M. (2009). Identification of equivalent material properties for 3-D numerical modeling of induction heating of ferromagnetic workpieces. IEEE Trans. Magnetics, 45(3), 1851-1854.